J. Fluid Mech. (2007), *vol.* 586, *pp.* 347–370.
doi:10.1017/S0022112007007100 Printed in the United Kingdom

On the boundary layer structure of differentially heated cavity flow in a stably stratified porous medium

P. G. DANIELS

Centre for Mathematical Science, City University, Northampton Square, London EC1V 0HB, UK

(Received 2 November 2006 and in revised form 20 April 2007)

This paper considers two-dimensional flow generated in a stably stratified porous medium by monotonic differential heating of the upper surface. For a rectangular cavity with thermally insulated sides and a constant-temperature base, the flow near the upper surface in the high-Darcy–Rayleigh-number limit is shown to consist of a double horizontal boundary layer structure with descending motion confined to the vicinity of the colder sidewall. Here there is a vertical boundary layer structure that terminates at a finite depth on the scale of the outer horizontal layer. Below the horizontal boundary layers the motion consists of a series of weak, uniformly stratified counter-rotating convection cells. Asymptotic results are compared with numerical solutions for the cavity flow at finite values of the Darcy–Rayleigh number.

1. Introduction

Owing to heating of the Earth's surface, many near-surface groundwater flows take place within a stably stratified environment which tends to inhibit motion. However, where uneven surface heating occurs, such as at the boundary between land and sea, horizontal differential heating can generate significant groundwater movement. An understanding of such motion can be important, for example, in judging the possible impact of industrial waste-water discharge into the sea (Tayler 1986). In the present paper a simple mathematical model is considered in which steady two-dimensional motion is generated within a stably stratified porous medium by differential heating of the upper surface. The main objectives are to determine the nature of the flow and temperature fields generated in the high-Darcy–Rayleigh-number limit and the depth to which motion extends.

Much of the previous work on thermally driven high-Darcy–Rayleigh-number flows is concerned with cavities heated from the side: the vertical boundary layer structure was first discussed by Weber (1975) and the horizontal boundary layer structure by Daniels, Blythe & Simpkins (1982). Similarity solutions of the horizontal boundary layer equations on a heated horizontal wall have been discussed by Cheng & Chang (1976) and Chang & Cheng (1983). More recently, the flow generated by differential heating of the upper surface of a rectangular cavity whose other three walls are thermally insulated has been considered by Daniels & Punpocha (2004; 2005) and Daniels (2006).

In the present work the flow is assumed to take place within a rectangular cavity with thermally insulated sidewalls and a lower surface held at constant temperature. The problem is formulated in § 2 and some numerical solutions are presented in § 3. Daniels

& Punpocha (2005) have shown that, for the case where the lower surface is thermally insulated, the main circulation takes place within horizontal and vertical boundary layers of depth order $R^{-1/3}$ near the upper surface, where $R \gg 1$ is the Darcy–Rayleigh number based on the cavity depth and the temperature difference along the upper surface. In that case, fluid moves along the upper surface to the colder end where it descends within a vertical boundary layer and is detrained back into the horizontal layer. The remainder of the cavity contains a weaker circulation, and is to leading order at a constant temperature somewhat greater than that of the colder end of the upper surface. In the present paper the temperature of the lower surface of the cavity is assumed to be held less than this value, with the consequence that the core is replaced by a stably stratified region of almost negligible motion. In addition, a new double horizontal/vertical boundary layer structure occurs near the upper surface. The inner horizontal layer of depth order $R^{-1/3}$ is similar to that of the insulated problem analysed by Daniels & Punpocha (2005), and is considered in § 4. The outer horizontal layer, which has depth of order $R^{-1/4}$, is considered in § 5 and is needed to allow the temperature field to adjust to its stably stratified form in the core region below. An interesting feature of this adjustment is that the vertical boundary layer near the colder sidewall terminates at a finite depth measured on the scale of the $R^{-1/4}$ layer. The terminal structure is considered in § 6 and the main results of the paper are summarized in § 7.

2. Formulation

A rectangular two-dimensional cavity $0 \leqslant x^* \leqslant d$, $0 \leqslant z^* \leqslant h$ is filled with a fluid-saturated porous medium. The upper boundary $z^* = h$ is held at temperature

$$T^* = T_0^* + \Delta T S(x^*/d), \tag{2.1}$$

where the function $S(x^*/d)$ varies monotonically from zero at $x^* = 0$ to 1 at $x^* = d$. The vertical walls $x^* = 0$ and $x^* = d$ are thermally insulated and the lower boundary $z^* = 0$ is held at temperature

$$T^* = T_0^* + \tau \Delta T, \tag{2.2}$$

where τ is a constant. Subject to Darcy's law and the Oberbeck–Boussinesq approximation, steady two-dimensional motion is governed by the non-dimensional equations

$$\nabla^2 \psi = -R \frac{\partial T}{\partial x}, \quad \nabla^2 T = \frac{\partial (T, \psi)}{\partial (x, z)}, \tag{2.3}$$

where $\psi(x, z)$ is the streamfunction non-dimensionalized by the thermal diffusivity κ, $T(x, z)$ is the temperature measured relative to T_0^* and non-dimensionalized by ΔT, (x, z) are Cartesian coordinates non-dimensionalized by h, and $R = Kg\omega \Delta T h/\kappa \nu$ is the Darcy–Rayleigh number, where K is the permeability, ω is the coefficient of thermal expansion, ν is the kinematic viscosity and g is the acceleration due to gravity. The non-dimensional velocity components in the x, z directions are given by $u = \partial \psi/\partial z$, $w = -\partial \psi/\partial x$ respectively.

The cavity walls are assumed to be impermeable so that the boundary conditions are

$$\psi = \frac{\partial T}{\partial x} = 0 \ \text{ on } x = 0, L, \tag{2.4}$$

$$\psi = 0, \quad T = \tau \ \text{ on } z = 0, \tag{2.5}$$

$$\psi = 0, \quad T = S(x/L) \ \text{ on } z = 1. \tag{2.6}$$

Solutions of the problem defined by (2.3)–(2.6) depend on the Darcy–Rayleigh number R and the aspect ratio $L = d/h$, and also on τ and the specific form of the temperature profile $S(x/L)$ at the upper surface, which is taken to be

$$S(x/L) = 1 - \left(1 - \frac{x}{L}\right)^2. \tag{2.7}$$

Apart from being a monotonic function, the precise form of S is not expected to have a significant impact on the large-Darcy–Rayleigh-number structure of the solution; the form (2.7) is chosen to enable comparison with previous results (Daniels & Punpocha 2005).

Note that because the sidewalls of the cavity are thermally insulated, it follows that the heat-flux integral

$$\int_0^L \left(\frac{\partial T}{\partial z} - \psi \frac{\partial T}{\partial x}\right) \mathrm{d}x = H \tag{2.8}$$

is constant for all values of z. In particular, H defines the heat flux into and out of the upper and lower surfaces of the cavity respectively, and is to be determined as part of the solution.

3. Numerical solutions

Numerical solutions of (2.3)–(2.7) were computed by inserting artificial time derivatives $\partial\psi/\partial t$ and $\partial T/\partial t$ on the right-hand sides of (2.3) and allowing the solution to evolve to its steady-state form. An explicit finite difference scheme was used with a forward difference in time and second-order accurate central differences in x and z. Quadratic extrapolation based on two internal grid points was used to implement the boundary conditions on $\partial T/\partial x$ at $x = 0$ and $x = L$. Solutions were computed to high spatial accuracy using step sizes Δx and Δz of 0.01, 0.005 and 0.0025, with time steps Δt in the range 2×10^{-5} to 10^{-6} to maintain numerical stability. A selection of results for a square cavity ($L = 1$) is shown in figures 1–3. For a potentially unstable case where the bottom wall temperature is equal to the maximum temperature of the upper surface ($\tau = 1$) a steady-state solution is obtained for R as high as 2000 (figure 1) and indicates the development of a complex thermal structure with significant variations near all four boundaries. For the stable case with $\tau = -1$, steady-state solutions can be obtained in principle for ever-increasing values of R; results for $R = 2000$ and $R = 5000$ are shown in figures 2 and 3 respectively. These indicate well-defined regions of circulation near the upper surface of the cavity, with the lower part dominated by a uniform stratification and an extremely weak set of counter-rotating cells which increase in number as R increases. The centre of the main recirculation zone approaches the upper cold corner of the cavity as R increases.

Figure 4 shows the solution for $\tau = 0.213$ and $R = 1000$. In this case the solution consists of a single-cell circulation with an almost-constant temperature core, and is similar to that obtained with an insulated lower boundary (Daniels & Punpocha 2004). In fact for the upper surface profile (2.7), $\tau_c = 0.213$ is a critical value of τ for high-Darcy–Rayleigh-number flows: for $\tau > \tau_c$ the flow appears to enter a complex and potentially unstable regime for sufficiently high values of R, whereas for $\tau < \tau_c$ it enters the stably stratified regime typified by the results of figures 2 and 3. For $\tau = \tau_c$, the structure described by Daniels & Punpocha (2005) is recovered to leading order as $R \to \infty$. The main aim of the present paper is to describe the asymptotic structure

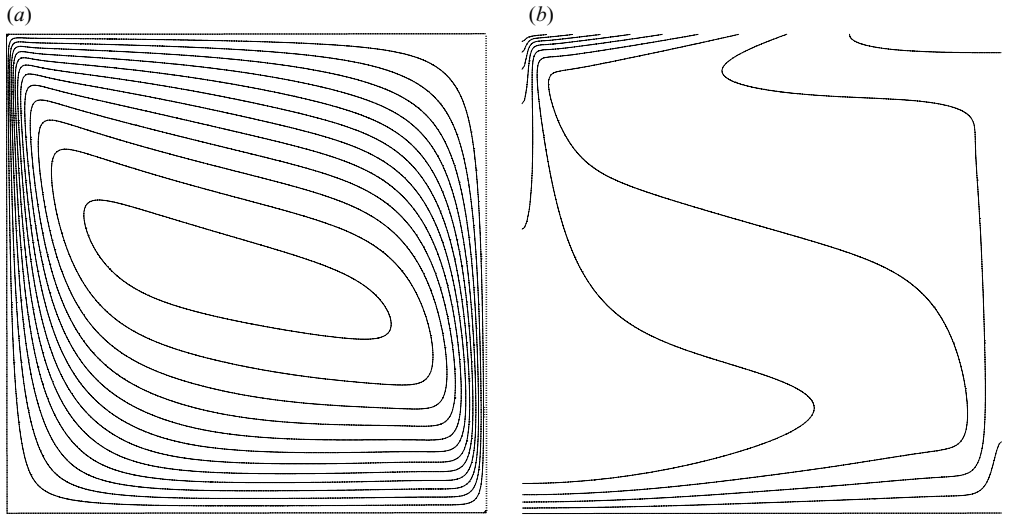

FIGURE 1. (*a*) Streamlines and (*b*) isotherms of the steady-state numerical solution for $L=1, \tau=1$ and $R=2000$. The flow is in the anticlockwise direction and ψ and T are shown at intervals of 2 and 0.1 respectively.

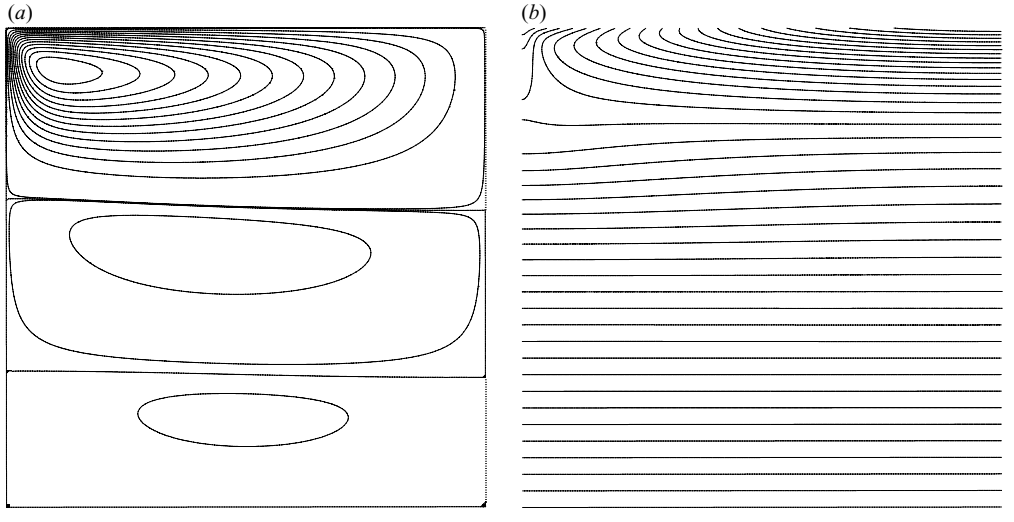

FIGURE 2. (*a*) Streamlines and (*b*) isotherms of the steady-state numerical solution for $L=1, \tau=-1$ and $R=2000$. The flow direction alternates, with the upper cell in the anticlockwise direction and values of ψ shown at intervals of 0.5 from 0 to 6; the streamlines shown in the lower cells are $\psi=-0.1, -0.005$ and 0.005. The isotherms are shown at intervals of 0.05.

of the more general class of high-Darcy–Rayleigh-number flows for which $\tau < \tau_c$. A schematic diagram of the proposed structure is shown in figure 5.

4. Inner horizontal boundary layer

A starting point for consideration of the high-Darcy–Rayleigh-number structure is the neighbourhood of the upper surface of the cavity (figure 5, region I), where the

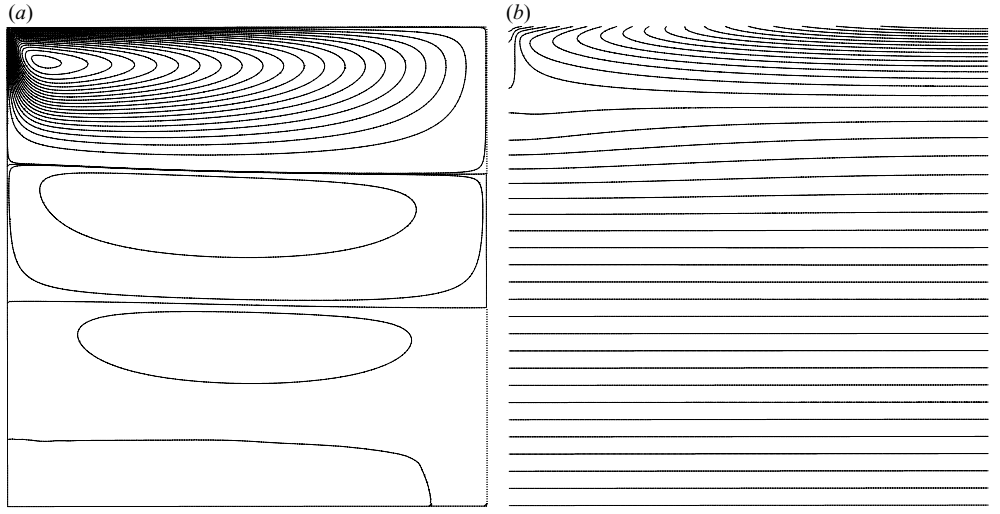

FIGURE 3. (*a*) Streamlines and (*b*) isotherms of the steady-state numerical solution for $L = 1, \tau = -1$ and $R = 5000$. The flow direction alternates, with the upper cell in the anticlockwise direction and values of ψ shown at intervals of 0.5 from 0 to 10; the streamlines in the lower cells are $\psi = -0.1, -0.005$ and 0.005. The isotherms are shown at intervals of 0.05.

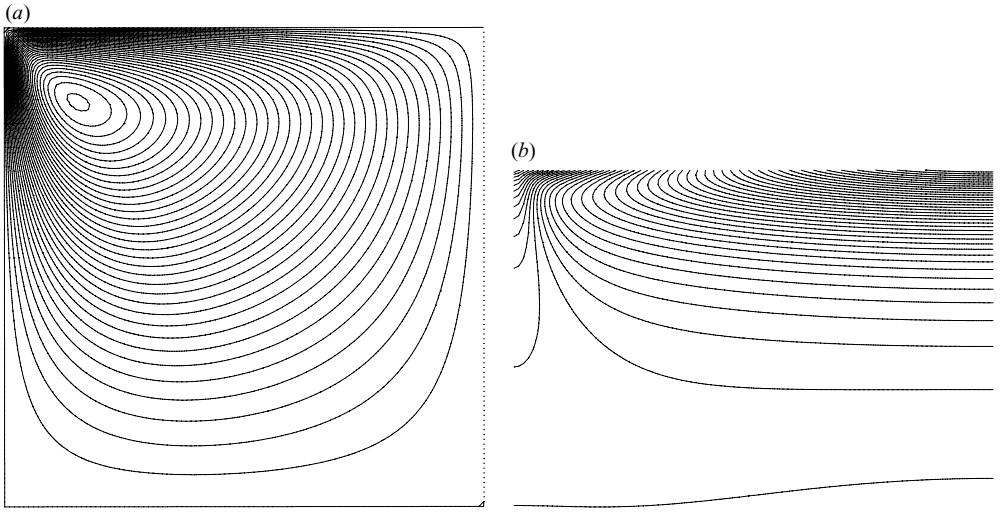

FIGURE 4. (*a*) Streamlines and (*b*) isotherms of the steady-state numerical solution for $L = 1, \tau = 0.213$ and $R = 1000$. The flow is in the anticlockwise direction and ψ and T are shown at intervals of 0.2 and 0.02 respectively.

flow is driven by the temperature profile (2.7). Locally the solution can be expanded in the form

$$T(x, z) = \bar{\theta}(X, Z) + \cdots, \quad \psi(x, z) = R^{1/3} L^{1/3} \bar{\phi}(X, Z) + \cdots, \tag{4.1}$$

where $x = LX$, $1 - z = R^{-1/3} L^{2/3} Z$ and $\bar{\theta}$ and $\bar{\phi}$ satisfy the equations

$$\frac{\partial^2 \bar{\phi}}{\partial Z^2} = -\frac{\partial \bar{\theta}}{\partial X}, \quad \frac{\partial^2 \bar{\theta}}{\partial Z^2} = \frac{\partial(\bar{\phi}, \bar{\theta})}{\partial(X, Z)}, \tag{4.2}$$

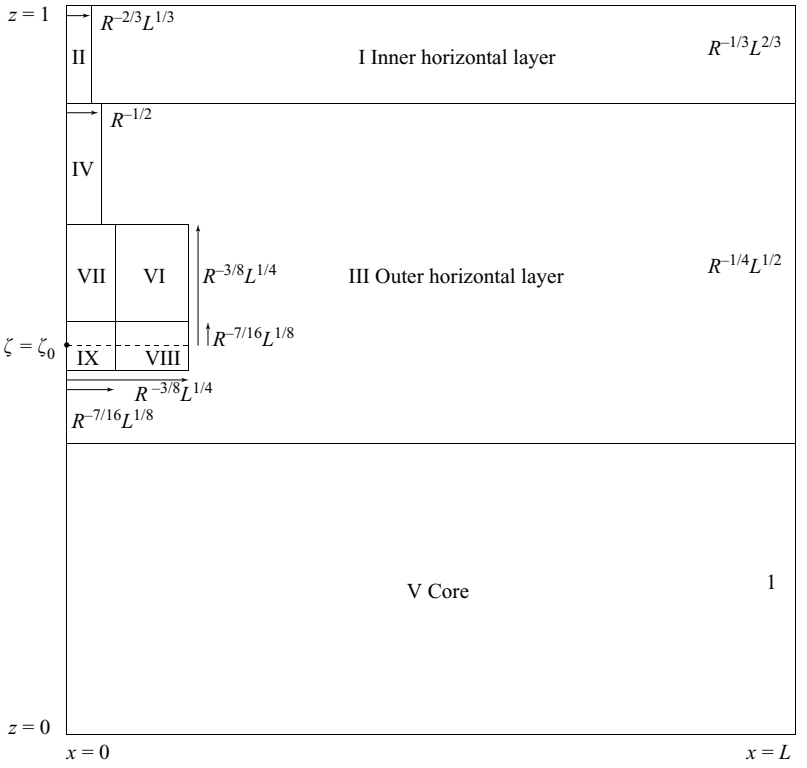

FIGURE 5. Schematic diagram of the flow structure in the large-Darcy–Rayleigh-number limit for $\tau < \tau_c$. The regions shown are the inner horizontal boundary layer (I) and vertical boundary layer (II), outer horizontal boundary layer (III) and vertical boundary layer (IV), core (V), convective zone (VI), conductive sublayer (VII), transitional layer (VIII) and sublayer extension (IX). The orders of magnitude of the dimensions of each region as $R \to \infty$ are indicated.

with boundary conditions

$$\bar{\phi} = 0, \quad \bar{\theta} = 1 - (1 - X)^2 \ \text{ on } Z = 0, \tag{4.3}$$

$$\bar{\phi} = \frac{\partial \bar{\theta}}{\partial X} = 0 \ \text{ on } X = 1, \tag{4.4}$$

$$\bar{\phi} \to 0, \quad \frac{\partial \bar{\theta}}{\partial Z} \to 0 \ \text{ as } Z \to \infty. \tag{4.5}$$

Here (4.3) are the conditions at the upper surface whilst (4.4) assumes that the boundary conditions at the hotter sidewall apply directly to the horizontal boundary layer solution. The conditions (4.5) at the bottom edge of the layer assume that the main circulation (of order $R^{1/3}$ in the streamfunction) is completed within the layer and that the temperature approaches a constant value to be determined.

At the colder sidewall there is a vertical boundary layer (figure 5, region II) which entrains fluid from the horizontal layer. Here

$$T(x, z) = \bar{\Theta}(\bar{\xi}, Z) + \cdots, \quad \psi(x, z) = R^{1/3} L^{1/3} \bar{\Phi}(\bar{\xi}, Z) + \cdots, \tag{4.6}$$

where $x = R^{-2/3}L^{1/3}\bar{\xi}$ and $\bar{\Theta}$ and $\bar{\Phi}$ satisfy the equations

$$\frac{\partial^2\bar{\Phi}}{\partial\bar{\xi}^2} = -\frac{\partial\bar{\Theta}}{\partial\bar{\xi}}, \quad \frac{\partial^2\bar{\Theta}}{\partial\bar{\xi}^2} = \frac{\partial(\bar{\Phi},\bar{\Theta})}{\partial(\bar{\xi},Z)} \tag{4.7}$$

and boundary conditions

$$\bar{\Phi} = \bar{\Theta} = 0 \ \text{ on } Z = 0, \tag{4.8}$$

$$\bar{\Phi} = \frac{\partial\bar{\Theta}}{\partial\bar{\xi}} = 0 \ \text{ on } \bar{\xi} = 0, \tag{4.9}$$

$$\bar{\Phi} \to \bar{\Phi}_\infty(Z), \quad \bar{\Theta} \to \bar{\Theta}_\infty(Z) \ \text{ as } \bar{\xi} \to \infty. \tag{4.10}$$

The edge profiles $\bar{\Phi}_\infty$ and $\bar{\Theta}_\infty$ are determined as part of the solution and must match with the solution in the horizontal layer, requiring that

$$\bar{\Phi}_\infty(Z) = \bar{\phi}(0,Z), \quad \bar{\Theta}_\infty(Z) = \bar{\theta}(0,Z). \tag{4.11}$$

In fact the interaction problem defined by (4.2)–(4.5) and (4.7)–(4.11) is identical to that solved by Daniels & Punpocha (2005) in their treatment of the cavity with a thermally insulated lower surface; in other words, the boundary condition at the lower wall does not influence the solution near the upper surface at this level of approximation. Confirmation of this can be seen from the heat-flux integral (2.8). In the insulating case $H = \int_0^L \partial T/\partial z(x,0)\mathrm{d}x = 0$, while in the present case with $\tau < \tau_c$ an order-one adjustment in temperature is needed over an order-one depth, suggesting that H remains finite (but non-zero) as $R \to \infty$. However, since contributions to the left-hand side of (2.8) from the horizontal boundary layer are of order $R^{1/3}$, this change in H has no impact on the leading-order solution there, which therefore satisfies

$$\int_0^1 \frac{\partial\bar{\theta}}{\partial Z}(X,0)\mathrm{d}X = 0 \tag{4.12}$$

at the upper surface, as in the insulating case.

Numerical and asymptotic solutions of (4.2)–(4.5) and (4.7)–(4.11) reported by Daniels & Punpocha (2005) show that the temperature profile in (4.3) drives a two-way flow in the horizontal boundary layer which is entrained and detrained by the vertical boundary layer. As $Z \to \infty$, the solutions in the horizontal and vertical boundary layers assume the algebraically decaying forms

$$\bar{\phi} \sim Z^{-1}p(X), \quad \bar{\theta} \sim b + Z^{-3}q(X), \tag{4.13}$$

where b is a constant and

$$\bar{\Phi} \sim Z^{-1}F_0(\bar{\eta}), \quad \bar{\Theta} \sim b + Z^{-3}G_0(\bar{\eta}), \tag{4.14}$$

where $\bar{\eta} = \bar{\xi}/Z^2$. Graphs of the functions p, q, F_0 and G_0 are given by Daniels & Punpocha (2005) (see also § 5.1 below). A correction to these asymptotic forms arises through the possibility of an origin shift in Z, equivalent to replacing Z by $Z + D$. Values of b and D are determined from the numerical solution of the overall combined boundary layer system and for the quadratic temperature profile in (4.3) are found to be $b = \tau_c = 0.213$ and $D = 3.70$ (Daniels & Punpocha 2005).

In the insulating problem b is the leading-order temperature of the core. Here, however, the temperature field in the core (figure 5, region V) must satisfy the condition (2.5) at $z = 0$ and matching with (4.13) at $z = 1$ implies the

conduction-dominated solution

$$T(x,z) = (\tau + \lambda z) + o(1), \quad \psi(x,z) = o(1) \tag{4.15}$$

as $R \to \infty$, where the stratification parameter

$$\lambda = b - \tau = \tau_c - \tau \tag{4.16}$$

is assumed to be positive. Thus, from (2.8), $H \to \lambda L$ as $R \to \infty$. It might appear that the z-dependence of the temperature field in (4.15) could match with a correction of order $R^{-1/3}$ to the temperature field within the inner horizontal layer. However, the core solution does not match directly as $z \to 1-$ with the algebraic decay of the horizontal boundary layer solution (4.13) as $Z \to \infty$. This would require an order-one streamfunction ψ within the core region depending on both x and z, and since the order-one core temperature must satisfy $\partial T/\partial x = 0$ and be consistent with (2.8) (leading to the linear form in z given in (4.15)) it follows from the heat equation in (2.3) that $\partial\psi/\partial x = 0$, contradicting the assertion that ψ is a finite function of both x and z. Instead, the core streamfunction is small as $R \to \infty$, and an outer horizontal layer exists where the vertical thermal gradients in the inner horizontal layer and core become comparable, requiring that $R^{1/3}Z^{-4} \sim 1$, or $1 - z \sim R^{-1/4}$. This outer horizontal boundary layer is considered next.

5. Outer horizontal boundary layer

In the outer horizontal layer (figure 5, region III) the solution can be expanded in the form

$$T(x,z) = b + R^{-1/4}L^{1/2}\theta(X,\zeta) + \cdots, \quad \psi(x,z) = R^{1/4}L^{1/2}\phi(X,\zeta) + \cdots, \tag{5.1}$$

as $R \to \infty$, where

$$1 - z = R^{-1/4}L^{1/2}\zeta - R^{-1/3}L^{2/3}D \tag{5.2}$$

and θ and ϕ satisfy the equations

$$\frac{\partial^2\phi}{\partial\zeta^2} = -\frac{\partial\theta}{\partial X}, \quad \frac{\partial^2\theta}{\partial\zeta^2} = \frac{\partial(\phi,\theta)}{\partial(X,\zeta)}, \tag{5.3}$$

with boundary conditions

$$\phi = \frac{\partial\theta}{\partial X} = 0 \ \text{ on } \ X = 1, \tag{5.4}$$

$$\phi \sim \zeta^{-1}p(X), \quad \theta \sim \zeta^{-3}q(X) \ \text{ as } \ \zeta \to 0, \tag{5.5}$$

$$\phi \to 0, \quad \theta \sim -\lambda\zeta \ \text{ as } \ \zeta \to \infty. \tag{5.6}$$

Here it is assumed that a solution can be found consistent with the wall conditions at $X = 1$, and (5.5) and (5.6) represent matching with the inner horizontal layer and core region respectively. In (5.2) the origin shift D is incorporated in the definition of ζ.

At the cold endwall the solution must match with that in a vertical boundary layer (figure 5, region IV). Here

$$T(x,z) = b + R^{-1/4}L^{1/2}\Theta(\xi,\zeta) + \cdots, \quad \psi(x,z) = R^{1/4}L^{1/2}\Phi(\xi,\zeta) + \cdots, \tag{5.7}$$

where $x = R^{-1/2}\xi$ and Θ and Φ satisfy the equations

$$\frac{\partial^2 \Phi}{\partial \xi^2} = -\frac{\partial \Theta}{\partial \xi}, \quad \frac{\partial^2 \Theta}{\partial \xi^2} = \frac{\partial(\Phi, \Theta)}{\partial(\xi, \zeta)}, \tag{5.8}$$

with boundary conditions

$$\Phi = \frac{\partial \Theta}{\partial \xi} = 0 \text{ on } \xi = 0, \tag{5.9}$$

$$\Phi \sim \zeta^{-1} F_0(\eta), \quad \Theta \sim \zeta^{-3} G_0(\eta) \text{ as } \zeta \to 0, \tag{5.10}$$

$$\Phi \to \Phi_\infty(\zeta), \quad \Theta \to \Theta_\infty(\zeta) \text{ as } \xi \to \infty, \tag{5.11}$$

where $\eta = \xi/\zeta^2$. Here (5.9) are the wall conditions and (5.10) represent matching with the vertical boundary layer associated with the inner horizontal layer. The edge profiles Φ_∞ and Θ_∞ are to be determined as part of the solution and must match with the solution in the outer horizontal layer, requiring that

$$\Phi_\infty(\zeta) = \phi(0, \zeta), \quad \Theta_\infty(\zeta) = \theta(0, \zeta) \text{ for } \zeta < \zeta_0. \tag{5.12}$$

Here ζ_0 is to be determined and defines the terminal point of the vertical boundary layer. This corresponds to the point at which the external streamfunction Φ_∞ reaches zero, $\Phi_\infty(\zeta_0) = 0$. Alternative structures corresponding to a gradual approach of Φ_∞ and $\Theta_\infty - \Theta_\infty(\infty) + \lambda\zeta$ to zero as $\zeta \to \infty$ appear not to be possible, because from (5.8) perturbations $\epsilon\hat{\Phi}$ and $\epsilon\hat{\Theta}$ in the vertical boundary layer would satisfy the system $\hat{\Phi}_{\xi\xi} = -\hat{\Theta}_\xi$, $\hat{\Theta}_{\xi\xi} = -\lambda\hat{\Phi}_\xi$ and there is no non-trivial solution satisfying the wall conditions $\hat{\Phi} = \hat{\Theta}_\xi = 0$ at $\xi = 0$ with finite behaviour as $\xi \to \infty$.

For $\zeta < \zeta_0$ the solution of the horizontal boundary layer has the form

$$\phi = \phi_0(\zeta) + X\phi_1(\zeta) + \cdots, \quad \theta = \theta_0(\zeta) + X\theta_1(\zeta) + \cdots, \tag{5.13}$$

as $X \to 0$, where $\phi_0 = \Phi_\infty$ and $\theta_0 = \Theta_\infty$, and it follows from (5.3) that

$$\theta_1 = -\phi_0'', \quad \phi_1 = (\theta_0'' - \phi_0'\phi_0'')/\theta_0'. \tag{5.14}$$

The expansions (5.13) must be modified near $\zeta = \zeta_0$ and the local structure there is considered in § 5.2 below.

For $\zeta > \zeta_0$ it is assumed that the solution in the outer horizontal layer satisfies the wall conditions directly, so that

$$\phi = \frac{\partial \theta}{\partial X} = 0 \text{ on } X = 0 \quad \text{for } \zeta > \zeta_0. \tag{5.15}$$

An expansion of the form (5.13) is still valid as $X \to 0$, but here $\phi_0 = \theta_1 = 0$, so that $\theta_0'' - \phi_1\theta_0' = 0$. Using the conditions (5.6) it follows that

$$\theta_0' = -\lambda \exp\left(-\int_\zeta^\infty \phi_1 \mathrm{d}\zeta\right), \quad \zeta > \zeta_0. \tag{5.16}$$

Now $-\phi_1$ is the scaled vertical slip velocity at the wall below ζ_0. Figure 3 suggests that this is weak and alternates in sign but is largest in the clockwise circulation immediately below ζ_0. Then the exponent in (5.16) is positive at $\zeta = \zeta_0$, and so

$$-\theta_0' \to \lambda_0 \equiv \lambda \exp\left(-\int_{\zeta_0}^\infty \phi_1 \mathrm{d}\zeta\right) > \lambda \quad \text{as } \zeta \to \zeta_0+. \tag{5.17}$$

This means that the vertical thermal gradient at the wall increases slightly from the value λ to the value λ_0 as $\zeta \to \zeta_0+$. This is consistent with a slight narrowing of the isotherms in this region in figure 3.

The proposed structure is now investigated in more detail by finding asymptotic solutions of the system in the limits $\zeta \to 0$, $\zeta \to \zeta_0$ and $\zeta \to \infty$. In this regard, it is first useful to note that the heat flux integral (2.8) taken across the outer horizontal layer and the vertical boundary layer implies that

$$\int_{X=0}^{1} \left(\frac{\partial \theta}{\partial \zeta} + \phi \frac{\partial \theta}{\partial X} \right) \mathrm{d}X + \int_{\xi=0}^{\infty} \Phi \frac{\partial \Theta}{\partial \xi} \mathrm{d}\xi = -\lambda \tag{5.18}$$

for all $\zeta > 0$, where the constant on the right-hand side has been evaluated using (5.6); the integral in ξ across the vertical boundary layer makes no contribution for $\zeta > \zeta_0$.

5.1. *Limiting structure, $\zeta \to 0$*

In the outer horizontal layer,

$$\phi = \zeta^{-1} p(X) + \zeta^3 P(X) + \cdots, \quad \theta = \zeta^{-3} q(X) + \zeta Q(X) + \cdots, \tag{5.19}$$

as $\zeta \to 0$, where the leading terms are those generated by the inner horizontal layer and the correction terms are needed to satisfy the integral condition (5.18). This is the first evidence that the thermal gradient in the core has an impact on the solution near the upper surface of the cavity. Note also that a constant contribution can be added in the temperature expansion (5.19) (and in the corresponding vertical layer expansion in (5.26) below) reflecting the fact that in the outer layer system (5.3)–(5.6), (5.8)–(5.12) and (5.15), the temperature is indeterminate to within an arbitrary constant. This constant represents the possibility of a correction (of order $R^{-1/4}$) to b but would only be present if a correction to the temperature of this magnitude were generated within the inner layer. Substitution of (5.19) into (5.3) gives

$$2p = -q', \quad 12q = pq' - 3p'q \tag{5.20}$$

and the solution found by Daniels & Punpocha (2005) is

$$p(X) = (12 q_0 v)^{1/2} (v + 1 - \alpha^2), \quad q(X) = q_0 (v + 1 - \alpha^2)^3, \tag{5.21}$$

where v is given implicitly as a function of X by the formula

$$X = 1 - (q_0 v/12)^{1/2} (v + 3 - 3\alpha^2), \quad 0 < v < \alpha^2 \tag{5.22}$$

and

$$q_0 = 4\alpha^{-2} (1 - 2\alpha^2/3)^{-2}/3. \tag{5.23}$$

The value of the constant α is determined by the solution in the vertical boundary layer (see (5.26)–(5.28) below) as $\alpha = F_0(\infty)/(12 q_0)^{1/2} = \mu_0/2\sqrt{3} = 0.750$, and this gives $q_0 = q(0) = 6.068$ and $p(0) = p_0 = 2\sqrt{3}\alpha q_0^{1/2} = 6.400$. The functions p and q are monotonically decreasing in X, with $p(1) = q'(1) = 0$ and $q(1) = 0.508$.

The equations for the correction terms P and Q are

$$6P = -Q', \quad 0 = pQ' + p'Q - 3(Pq' + P'q) \tag{5.24}$$

and the solutions satisfying the boundary conditions $P(1) = Q'(1) = 0$ are

$$Q = \mu q, \quad P = \mu p/3, \tag{5.25}$$

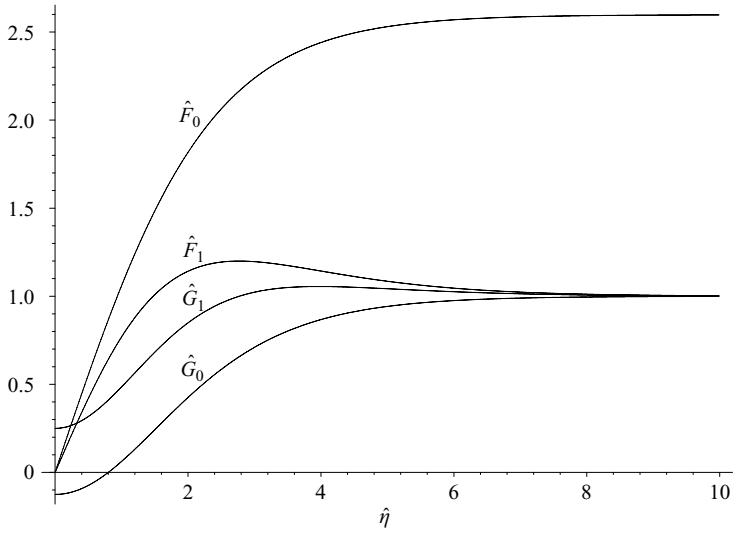

FIGURE 6. Functions $\hat{F}_0, \hat{G}_0, \hat{F}_1, \hat{G}_1$ involved in the vertical boundary layer solution as $\zeta \to 0$.

where μ is an arbitrary constant. Note that a solution with $Q = -\lambda$ is not possible, confirming that the core temperature gradient in (4.15) cannot match directly with the solution in the inner horizontal layer.

In the vertical boundary layer,

$$\Phi = \zeta^{-1} F_0(\eta) + \zeta^3 F_1(\eta) + \cdots, \quad \Theta = \zeta^{-3} G_0(\eta) + \zeta G_1(\eta) + \cdots, \tag{5.26}$$

where $\eta = \xi/\zeta^2$. Substitution into (5.8) shows that the solutions for the leading terms can be written as

$$F_0 = q_0^{1/2} \hat{F}_0(\hat{\eta}), \quad G_0 = q_0 \hat{G}_0(\hat{\eta}), \tag{5.27}$$

where $\hat{\eta} = q_0^{1/2}\eta$, $\hat{G}_0 = 1 - \hat{F}_0'$ and $\hat{F}_0$ satisfies

$$\hat{F}_0''' - \hat{F}_0 \hat{F}_0'' + 3\hat{F}_0'(\hat{F}_0' - 1) = 0, \quad \hat{F}_0 = \hat{F}_0'' = 0, \hat{\eta} = 0, \quad \hat{F}_0' \to 0 \text{ as } \hat{\eta} \to \infty. \tag{5.28}$$

This has a non-trivial solution found by Daniels & Punpocha (2005) with $\hat{F}_0(\infty) = \mu_0 = 2.598$ and $\hat{F}_0'(0) = 1.125$. The values of p_0 and q_0 then follow from the relation $p_0 = \mu_0 q_0^{1/2}$ and (5.23).

The correction terms F_1 and G_1 can now be obtained in the form

$$F_1 = P_0 \hat{F}_1(\hat{\eta}), \quad G_1 = Q_0 \hat{G}_1(\hat{\eta}), \tag{5.29}$$

where $P_0 = P(0) = \mu p_0/3$, $Q_0 = Q(0) = \mu q_0$, $\hat{F}_1$ is the solution of the system

$$\hat{F}_1'' - \hat{F}_0 \hat{F}_1' + 3(\hat{F}_0' - 1)\hat{F}_1 = -3\mu_0^{-1} \hat{F}_0, \quad \hat{F}_1 = 0, \hat{\eta} = 0, \quad \hat{F}_1 \to 1 \text{ as } \hat{\eta} \to \infty \tag{5.30}$$

and $\hat{G}_1 = 1 - \mu_0 \hat{F}_1'/3$. The solutions for $\hat{F}_1$ and $\hat{G}_1$ obtained using a fourth-order Runge-Kutta scheme are shown along with $\hat{F}_0$ and $\hat{G}_0$ in figure 6, and in particular it was found that $\hat{F}_1'(0) = 0.866$.

The correction terms in both the horizontal boundary layer and the vertical boundary layer are now completely determined in terms of the single arbitrary parameter μ. This is determined finally by appeal to the heat flux condition (5.18). Making use of (5.25), the contributions to the left-hand side from the horizontal

boundary layer as $\zeta \to 0$ are

$$-\frac{3}{4}p_0q_0\zeta^{-4} + \mu\left(5\int_0^1 q\,\mathrm{d}X - p_0q_0\right) + o(1), \tag{5.31}$$

whilst the contributions from the vertical boundary layer are

$$\frac{3}{4}p_0q_0\zeta^{-4} + \frac{2}{3}\mu p_0q_0\int_0^\infty \hat{F}_0'\hat{F}_1'\mathrm{d}\hat{\eta} + o(1). \tag{5.32}$$

The leading terms cancel and the two integrals arising in the finite parts can be evaluated using the analytical form for q given in (5.21) and the numerical solutions for $\hat{F}_0$ and $\hat{F}_1$. Using $\alpha = \mu_0/2\sqrt{3}$, this gives

$$\int_0^1 q\,\mathrm{d}X = \frac{\sqrt{3q_0^3}}{4}\left(\frac{256}{315}\alpha^8 - \frac{128}{35}\alpha^6 + \frac{32}{5}\alpha^4 - \frac{16}{3}\alpha^2 + 2\right)\alpha = 2.211 \tag{5.33}$$

and $\int_0^\infty \hat{F}_0'\hat{F}_1'\mathrm{d}\hat{\eta} = 1.125$. It now follows from (5.18) that $\mu = -0.743\lambda$.

As $\zeta \to 0$, the edge profiles Φ_∞ and Θ_∞ have the forms

$$\Phi_\infty \sim 6.400\zeta^{-1}(1 + \tfrac{1}{3}\mu\zeta^4), \quad \Theta_\infty \sim 6.068\zeta^{-3}(1 + \mu\zeta^4), \tag{5.34}$$

whilst the wall temperature $\Theta_w = \Theta(0, \zeta)$ has the behaviour

$$\Theta_w \sim -0.759\zeta^{-3}(1 - 2\mu\zeta^4). \tag{5.35}$$

The effect of the positive gradient λ is thus to enhance the reduction of Φ_∞ and Θ_∞ and to diminish the increase of Θ_w as ζ increases. In fact use of (5.34) as an approximation at finite ζ predicts that Φ_∞ reaches zero when $\zeta = \zeta_0 = 1.418\lambda^{-1/4}$. It also predicts an inflection point of Φ_∞ corresponding to a local minimum of the horizontal detrainment velocity when $\zeta = 1.077\lambda^{-1/4}$. In addition, (5.34) and (5.35) predict that the wall temperature Θ_w reaches a maximum value, and coincides with the value of Θ_∞, when $\zeta = 1.192\lambda^{-1/4}$. The results (5.34), (5.35) are strictly valid only as $\zeta\lambda^{1/4} \to 0$, but provide a useful guide to how the thermal gradient λ affects the behaviour of the vertical boundary layer. It should be added that the correction terms in (5.19) and (5.26) of relative order ζ^4 are made necessary by the integral condition (5.18), which guarantees the appearance of the arbitrary constant μ in the combined horizontal/vertical boundary layer solution. Apart from the constant contribution to the temperature already discussed, an assumption of possible larger corrections as $\zeta \to 0$ does not appear to lead to a consistent solution across both layers.

5.2. *Limiting structure, $\zeta \to \zeta_0$*

The structure to be discussed here is based on the conjecture that, near the cold sidewall, the transition to a stratified flow with no wall entrainment occurs abruptly near ζ_0. Suppose that Φ_∞ and Θ_∞ both approach the point ζ_0 in a linear fashion, so that

$$\Phi_\infty = a_1(\zeta_0 - \zeta) + a_2(\zeta_0 - \zeta)^2 + \cdots, \quad \Theta_\infty = b_0 + b_1(\zeta_0 - \zeta) + b_2(\zeta_0 - \zeta)^2 + \cdots, \tag{5.36}$$

as $\zeta \to \zeta_0-$, where $a_1 > 0$ and $b_1 \geqslant 0$. In the horizontal boundary layer there is a transition region as $X \to 0$ where

$$\phi = X^{1/2}f_0(\beta) + Xf_1(\beta) + \cdots, \quad \theta = b_0 + X^{1/2}g_0(\beta) + Xg_1(\beta) + \cdots \tag{5.37}$$

and $\beta = (\zeta_0 - \zeta)/X^{1/2}$ which allows the linear forms to be modified. The leading-order functions f_0 and g_0 satisfy the equations

$$f_0'' = \tfrac{1}{2}(\beta g_0' - g_0), \quad g_0'' = \tfrac{1}{2}(g_0f_0' - g_0'f_0), \tag{5.38}$$

with boundary conditions $f_0' \to a_1$, $g_0' \to b_1$ as $\beta \to \infty$ and below ζ_0 the stratified flow with no entrainment is equivalent to the behaviour $f_0' \to 0$, $g_0' \to \lambda_0$ as $\beta \to -\infty$. By converting this into a coupled system for f_0 and $g_0 - \lambda_0\beta + \lambda_0^{1/2} f_0$, it can be shown that solutions have the form

$$g_0 = \lambda_0^{3/4}(\tilde{\beta} - \tilde{f}(\tilde{\beta})), \quad f_0 = \lambda_0^{1/4}\tilde{f}(\tilde{\beta}), \tag{5.39}$$

where $\tilde{\beta} = \lambda_0^{1/4}\beta$, and $\tilde{f}$ is the solution of

$$\tilde{f}'' + \frac{1}{2}(\tilde{\beta}\tilde{f}' - \tilde{f}) = 0, \quad \tilde{f}' \to 0,\ \tilde{\beta} \to -\infty, \quad \tilde{f}' \to 1 - \lambda_0^{-1}b_1,\ \tilde{\beta} \to \infty, \tag{5.40}$$

namely

$$\tilde{f} = (1 - \lambda_0^{-1}b_1)\left\{\frac{\tilde{\beta}}{2}\left(1 + \operatorname{erf}\frac{\tilde{\beta}}{2}\right) + \frac{1}{\sqrt{\pi}}e^{-\tilde{\beta}^2/4}\right\}. \tag{5.41}$$

For a given value of b_1, the value of a_1 cannot be specified arbitrarily, and is given by

$$a_1 = \lambda_0^{1/2}(1 - \lambda_0^{-1}b_1). \tag{5.42}$$

The solution of the nonlinear system (5.38) from the linear system (5.40) is an example of the interesting general result that for $\lambda_0 R > 0$ the nonlinear porous medium equations (2.3) admit solutions of the form $T = \lambda_0 z - (\lambda_0/R)^{1/2}\psi + \text{const.}$, provided that ψ is a solution of the linear system $\nabla^2\psi = (R\lambda_0)^{1/2}\psi_x$.

The above analysis shows that the horizontal boundary layer equations can facilitate an abrupt transition to a stratified state with thermal gradient λ_0 and zero entrainment provided the incoming thermal and streamfunction gradients are related by (5.42). The next step is to consider whether this structure is consistent with a solution of the vertical boundary layer. It is shown in the Appendix that in fact this requires $b_1 = 0$, and assuming that $b_2 \neq 0$, it follows that in the vertical boundary layer, as $\zeta \to \zeta_0-$,

$$\Phi = (\zeta_0 - \zeta)f(\delta) + \cdots, \quad \Theta = b_0 + (\zeta_0 - \zeta)^2 g(\delta) + \cdots, \tag{5.43}$$

where $\delta = \xi(\zeta_0 - \zeta)$ and f and g satisfy the convection-dominated system

$$f' = b_2 - g, \quad fg' - 2f'g = 0. \tag{5.44}$$

Thus $g = kf^2$, where k is a positive constant, $b_2 = ka_1^2$ and the solution for f which vanishes at $\delta = 0$ is

$$f = a_1 \tanh(a_1 k\delta). \tag{5.45}$$

Closer to the wall there is a sublayer where conduction is significant and

$$\Phi = (\zeta_0 - \zeta)^{3/2}F(\gamma) + \cdots, \quad \Theta = b_0 + (\zeta_0 - \zeta)^3 G(\gamma) + \cdots, \tag{5.46}$$

where $\gamma = \xi(\zeta_0 - \zeta)^{1/2}$. Here matching with (5.45) gives $F = a_1^2 k\gamma$ and G satisfies

$$G'' - \frac{3}{2}a_1^2 k\gamma G' + 3a_1^2 kG = 0, \quad G' = 0,\ \gamma = 0, \quad G \sim a_1^4 k^3 \gamma^2,\ \gamma \to \infty. \tag{5.47}$$

The required solution is

$$G = a_1^4 k^3 \gamma^2 - \tfrac{2}{3}a_1^2 k^2. \tag{5.48}$$

The quadratic dependence of temperature on streamfunction in the outer convective zone is essential to ensure the existence of an inner temperature field with zero heat transfer at the wall. Both the outer convective zone and the conductive sublayer spread away from the wall (with $\xi \sim (\zeta_0 - \zeta)^{-1}$ and $(\zeta_0 - \zeta)^{-1/2}$ respectively) so

that the vertical boundary layer width increases dramatically as $\zeta \to \zeta_0-$. The wall temperature has the behaviour

$$\Theta \sim b_0 - \tfrac{2}{3}a_1^2 k^2(\zeta_0 - \zeta)^3, \tag{5.49}$$

as $\zeta \to \zeta_0-$, indicating an approach to a maximum value at $\zeta = \zeta_0$. In this sense the structure of the vertical boundary layer described here is comparable with that suggested by the small-ζ analysis except that the zero of $\Theta_w - \Theta_\infty$, the maximum value of Θ_w and the zero of Φ_∞ are predicted to occur simultaneously at the terminal point ζ_0.

With $b_1 = 0$ for consistency within the vertical boundary layer, it now follows from (5.42) that

$$a_1 = -\Phi_\infty'(\zeta_0) = \lambda_0^{1/2}. \tag{5.50}$$

In practice, this condition must be satisfied through the interaction between the two layers. The finite value of $\Phi_\infty'(\zeta_0)$ confirms the initial assumption in (5.36) that Φ_∞ is linear in ζ as $\zeta \to \zeta_0$; vertical boundary layer structures for more general forms $\Phi_\infty \sim (\zeta_0 - \zeta)^n$ as $\zeta \to \zeta_0$ can be found which have a quadratic dependence of temperature on streamfunction in the outer convective zone, but these are not consistent with the limiting behaviour $\Phi_\infty \sim \lambda_0^{1/2}(\zeta_0 - \zeta)$ as $\beta \to \infty$ generated within the transition region of the horizontal boundary layer. The terminal condition (5.50) is used to obtain an approximate estimate of the value of ζ_0 in § 7 below.

It is now possible to return to the horizontal boundary layer and consider the second terms in the transition region expansion (5.37), the solutions for f_0 and g_0 being given by (5.39)–(5.42) with $b_1 = 0$ and $a_1 = \lambda_0^{1/2}$. The functions f_1 and g_1 satisfy the equations

$$f_1'' = \tfrac{1}{2}\beta g_1' - g_1, \quad g_1'' = f_0' g_1 - \tfrac{1}{2} f_0 g_1' + \tfrac{1}{2} g_0 f_1' - g_0' f_1 \tag{5.51}$$

and boundary conditions

$$f_1 \sim a_2\beta^2, \quad g_1 \sim b_2\beta^2 \ \text{ as } \beta \to \infty, \quad f_1 \to 0, \quad g_1 \to 0 \ \text{ as } \beta \to -\infty. \tag{5.52}$$

Here the conditions as $\beta \to \infty$ follow from matching with (5.13) whilst those as $\beta \to -\infty$ are equivalent to a requirement that $\theta_0''(\zeta_0+) = -\lambda_0\phi_1(\zeta_0+) = 0$, so that the upward slip velocity at the wall reaches zero just below the transition region. If it were non-zero then f_1 and g_1 would be finite and quadratic respectively as $\beta \to -\infty$, and by considering the second-order equation for $\lambda_0^{1/2} f_1 + g_1$ obtained from (5.51) it can be shown that there is then a linear term in β as $\beta \to \infty$ which cannot match with (5.13). The solution of (5.51), (5.52) can be written in the form

$$g_1 = -\tilde{f}_1(\tilde{\beta}), \quad f_1 = \lambda_0^{-1/2}\tilde{f}_1(\tilde{\beta}), \tag{5.53}$$

where $\tilde{f}_1$ satisfies

$$\tilde{f}_1'' + \frac{1}{2}\tilde{\beta}\tilde{f}_1' - \tilde{f}_1 = 0, \quad \tilde{f}_1 \sim a_2\tilde{\beta}^2, \ \tilde{\beta} \to \infty, \quad \tilde{f}_1 \to 0, \ \tilde{\beta} \to -\infty, \tag{5.54}$$

and it is required that

$$b_2 = -a_2\lambda_0^{1/2}. \tag{5.55}$$

Since $b_2 \geqslant 0$ this implies that $a_2 = \frac{1}{2}\Phi_\infty''(\zeta_0-) \leqslant 0$. This is consistent with the prediction of the small-ζ analysis that there is an inflection point in the solution for $\Phi_\infty(\zeta)$ ahead of the terminal point of the vertical boundary layer.

The solution for $\tilde{f}_1$ is

$$\tilde{f}_1 = 4a_2\pi^{-1/2}(\tilde{\beta}^2+2)\int_{-\infty}^{\tilde{\beta}}(\hat{\beta}^2+2)^{-2}\mathrm{e}^{-\hat{\beta}^2/4}\mathrm{d}\hat{\beta}. \tag{5.56}$$

The relation between b_2 and a_2 determined by (5.55) implies that $(\theta_0'' - \phi_0'\phi_0'')(\zeta_0) = 2(b_2 + a_1a_2) = 0$, so that although $b_1 = -\theta_0'(\zeta_0) = 0$ the outer function ϕ_1 in (5.13) is not singular as $\zeta \to \zeta_0-$. Note also that $\tilde{f}_1 \sim a_2\tilde{\beta}^2 + 2a_2$ as $\tilde{\beta} \to \infty$, and the absence of a linear term in $\tilde{\beta}$ is consistent with the fact that no term of order $X^{1/2}$ can be generated in the outer expansion (5.13).

5.3. *Limiting structure, $\zeta \to \infty$*

In the limit $\zeta \to \infty$ the horizontal boundary layer is dominated by uniform stratification and exponentially weak flow. An asymptotic solution of equations (5.3) subject to the end conditions (5.4) and (5.15) can be found by writing

$$\phi = \hat{\phi}(X,\zeta), \quad \theta = -\lambda\zeta + \hat{\theta}(X,\zeta) \tag{5.57}$$

and linearizing about the uniform stratification. Ignoring solutions that grow exponentially as $\zeta \to \infty$, the general solutions for $\hat{\phi}$ and $\hat{\theta}$ satisfying (5.4) and (5.15) are

$$\hat{\phi} = \sum_{n=1}^{\infty} r_n(\zeta)\sin n\pi X, \quad \hat{\theta} = \sum_{n=0}^{\infty} s_n(\zeta)\cos n\pi X, \tag{5.58}$$

where s_0 is constant and

$$r_n = (\alpha_n\cos\omega_n\zeta + \beta_n\sin\omega_n\zeta)\mathrm{e}^{-\omega_n\zeta}, \quad s_n = \frac{2\omega_n^2}{n\pi}(\alpha_n\sin\omega_n\zeta - \beta_n\cos\omega_n\zeta)\mathrm{e}^{-\omega_n\zeta}, \tag{5.59}$$

for $n = 1, 2, \ldots$, where $\omega_n = (n\pi\lambda^{1/2}/2)^{1/2}$. The Fourier coefficients α_n and β_n and the constant s_0 are not determined locally, and it should be recognized that for $n \geqslant 4$ the Fourier components identified here are of comparable magnitude to other terms in ϕ and θ arising from nonlinear products of the partial derivatives of $\hat{\phi}$ and $\hat{\theta}$. The results indicate the existence of exponentially weak counter-rotating cells of depth $\zeta \sim \pi/\omega_1 = \sqrt{2\pi}\lambda^{-1/4}$ as $\zeta \to \infty$. Note that algebraically decaying solutions for $\hat{\phi}$ and $\hat{\theta}$ as $\zeta \to \infty$ are not possible : the outer horizontal layer transforms the algebraic decay at the lower edge of the inner horizontal layer into the exponential decay needed to match with the core solution (4.15).

5.4. *Approximate solution*

By combining the results of § 5.1 and § 5.3 above, an approximate solution of the entire outer horizontal boundary layer can be constructed as follows. It is assumed that for $\zeta < \zeta_1$ (where ζ_1 is to be determined) the solution is represented by the leading terms of the small-ζ expansion (5.19), and that for $\zeta > \zeta_1$ it is represented by the large-ζ form (5.57)–(5.59) but with ζ replaced by $\zeta - \zeta_1$ for convenience. Continuity of ϕ and θ at $\zeta = \zeta_1$ then requires

$$\zeta_1^{-1}p(X) = \sum_{n=1}^{\infty}\alpha_n\sin n\pi X, \quad \zeta_1^{-3}q(X) = s_0 - 2\pi^{-1}\sum_{n=1}^{\infty}n^{-1}\beta_n\omega_n^2\cos n\pi X, \tag{5.60}$$

so that

$$\alpha_n = 2\zeta_1^{-1}I_n, \quad \beta_n = -n\pi\omega_n^{-2}\zeta_1^{-3}J_n, \quad s_0 = \zeta_1^{-3}J_0, \tag{5.61}$$

n	I_n	J_n
0		2.21110
1	1.70973	1.08841
2	1.03533	0.32952
3	0.67228	0.14262
4	0.50876	0.08093
5	0.40666	0.05174
6	0.33918	0.03595
7	0.29078	0.02641
8	0.25449	0.02021
9	0.22624	0.01596
10	0.20363	0.01293

TABLE 1. Values of I_n and J_n for n up to 10.

where

$$I_n = \int_0^1 p(X)\sin n\pi X \mathrm{d}X, \ \ n = 1, 2, \cdots, \quad J_n = \int_0^1 q(X)\cos n\pi X \mathrm{d}X, \ \ n = 0, 1, \cdots. \tag{5.62}$$

These integrals can be evaluated using the analytical forms (5.21) and a change of variable $V = v^{1/2}$, where v is defined by (5.22), to give

$$I_n = 3q_0 \int_0^\alpha V(V^2 + 1 - \alpha^2)^2 \sin\{n\pi(1 - (q_0/12)^{1/2}V(V^2 + 3 - 3\alpha^2)\}\mathrm{d}V, \tag{5.63}$$

$$J_n = (3q_0^3/4)^{1/2} \int_0^\alpha (V^2 + 1 - \alpha^2)^4 \cos\{n\pi(1 - (q_0/12)^{1/2}V(V^2 + 3 - 3\alpha^2)\}\mathrm{d}V. \tag{5.64}$$

Values of I_n and J_n are shown in table 1 for n up to 10. Note that for $n = 0$ the value of J_0 is consistent with the analytical formula (5.33). A value for ζ_1 can be obtained by requiring continuity of the mean vertical thermal gradient across the layer, $\int_0^1 \theta_\zeta(X, \zeta_1)\mathrm{d}X$, giving $\zeta_1 = (3J_0/\lambda)^{1/4}$. The approximate solution for $\zeta > \zeta_1$ is then

$$\phi = \sum_{n=1}^{\infty} (\alpha_n \cos\omega_n(\zeta - \zeta_1) + \beta_n \sin\omega_n(\zeta - \zeta_1))\mathrm{e}^{-\omega_n(\zeta - \zeta_1)} \sin n\pi X, \tag{5.65}$$

$$\theta = \lambda(\zeta_1 - \zeta) + \frac{J_0}{\zeta_1^3} + \sum_{n=1}^{\infty} \frac{2\omega_n^2}{n\pi}(\alpha_n \sin\omega_n(\zeta - \zeta_1) - \beta_n \cos\omega_n(\zeta - \zeta_1))\mathrm{e}^{-\omega_n(\zeta - \zeta_1)} \cos n\pi X. \tag{5.66}$$

The flow pattern predicted by a 10-mode approximation to ϕ in (5.65) is shown in figure 7 and can be compared with the numerical results of figures 2 and 3. The approximate solution reproduces the slight downward tilt of the dividing streamlines and quite accurately predicts their vertical separation $\zeta \sim \sqrt{2\pi}\lambda^{-1/4}$; the vertical scaling in figure 7 corresponds to $L = 1$, $R = 5000$ and $\lambda = b - \tau = 1.213$, allowing a direct comparison with figure 3. The approximate solution does not provide an accurate representation of the flow near the upper stagnation point on the cold endwall but this is not surprising because it does not incorporate the vertical boundary layer in the region just below ζ_1 or the local structure identified in § 5.2, including the terminal condition (5.50).

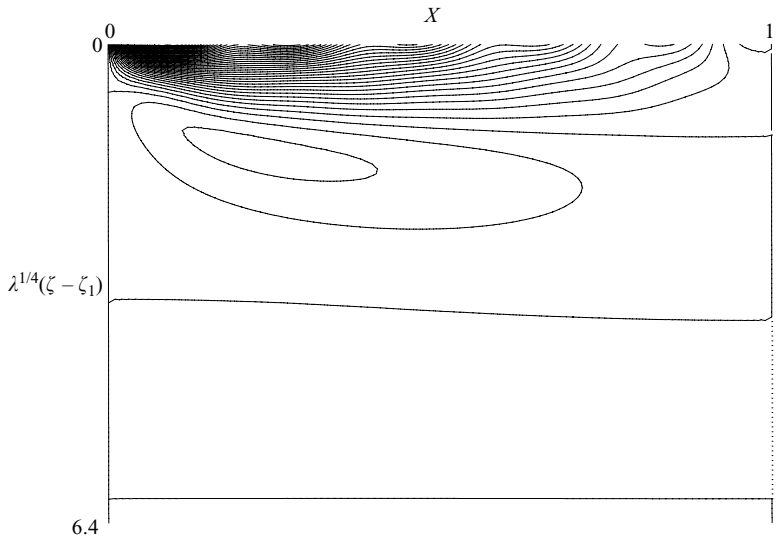

FIGURE 7. Approximate solution of the outer horizontal layer for $\zeta > \zeta_1$ showing the streamlines predicted by a 10-mode approximation to ϕ in (5.65). The vertical scale is chosen to correspond to the actual length scale in the cavity in the case where $L = 1$, $R = 5000$ and $\tau = -1$, allowing a direct comparison with the numerical solution of figure 3.

6. Vertical boundary layer terminal structure

The terminal form of the vertical boundary layer solution proposed in § 5.2 consists of an outer zone $\xi \sim (\zeta_0 - \zeta)^{-1}$ dominated by convection and an inner conduction zone $\xi \sim (\zeta_0 - \zeta)^{-1/2}$. In this section it is considered how this near-wall structure is modified close to ζ_0. As ζ approaches ζ_0 the width of the outer zone $x \sim R^{-1/2}\xi \sim R^{-1/2}(\zeta_0 - \zeta)^{-1}$ increases until it becomes comparable with the vertical scale of variation in z. This occurs in a convection-dominated zone (figure 5, region VI).

6.1. *Convective zone*

Here the local coordinates $\tilde{x}$ and $\tilde{\zeta}$ are defined by

$$x = R^{-3/8}L^{1/4}\lambda_0^{-1/4}\tilde{x}, \quad \zeta = \zeta_0 - R^{-1/8}L^{-1/4}\lambda_0^{-1/4}\tilde{\zeta}, \tag{6.1}$$

and the solution is

$$T = \{b + R^{-1/4}L^{1/2}b_0 + \cdots\} + R^{-1/2}\lambda_0^{1/2}\tilde{\Theta}(\tilde{x}, \tilde{\zeta}) + \cdots, \quad \psi = R^{1/8}L^{1/4}\lambda_0^{1/4}\tilde{\Phi}(\tilde{x}, \tilde{\zeta}) + \cdots, \tag{6.2}$$

where the terms in parentheses (and in (6.10), (6.14) and (6.25) below) are constant contributions to the temperature field. Substitution into (2.3) shows that $\tilde{\Theta}$ and $\tilde{\Phi}$ satisfy

$$\tilde{\nabla}^2\tilde{\Phi} = -\frac{\partial\tilde{\Theta}}{\partial\tilde{x}}, \quad \frac{\partial(\tilde{\Phi}, \tilde{\Theta})}{\partial(\tilde{x}, \tilde{\zeta})} = 0, \tag{6.3}$$

where $\tilde{\nabla}^2 = \partial^2/\partial\tilde{x}^2 + \partial^2/\partial\tilde{\zeta}^2$. Matching with the outer zone of the vertical boundary layer as $\tilde{\zeta} \to \infty$ implies that $\tilde{\Theta} = k\tilde{\Phi}^2$, and it follows that $\tilde{\Phi}$ is the solution of the

elliptic system

$$\tilde{\nabla}^2\tilde{\Phi} = -2k\tilde{\Phi}\frac{\partial\tilde{\Phi}}{\partial\tilde{x}}, \tag{6.4}$$

$$\tilde{\Phi} = 0 \quad \text{on } \tilde{x} = 0 \text{ and } \tilde{\zeta} = 0, \tag{6.5}$$

$$\tilde{\Phi} \sim \tilde{\zeta}\tanh(k\tilde{x}\tilde{\zeta}) \quad \text{as } \tilde{\zeta} \to \infty, \tag{6.6}$$

$$\tilde{\Phi} \sim \tilde{\zeta} \quad \text{as } \tilde{x} \to \infty. \tag{6.7}$$

Here the conditions (6.5) on $\tilde{x} = 0$ and $\tilde{\zeta} = 0$ follow from matching with the solutions in a conductive sublayer and a transitional zone (respectively) to be discussed below, (6.6) follows from matching with the vertical boundary layer and (6.7) from matching with the outer horizontal boundary layer (where the boundary layer constant a_1 has been replaced in terms of λ_0 using (5.50)). Inclusion of the thermal gradient λ_0 in the scalings (6.1) and (6.2) allows this parameter to be removed from the system (6.4)–(6.7).

As $\tilde{x} \to 0$ it can be expected that $\tilde{\Phi} \sim W(\tilde{\zeta})\tilde{x}$, where the slip velocity $W(\tilde{\zeta})$ has the asymptotic behaviours

$$W \sim k\tilde{\zeta}^2, \ \tilde{\zeta} \to \infty, \quad W \sim W_0\tilde{\zeta}, \ \tilde{\zeta} \to 0, \tag{6.8}$$

with $W_0 > 0$. Similarly, as $\tilde{\zeta} \to 0$ it can be expected that $\tilde{\Phi} \sim U(\tilde{x})\tilde{\zeta}$, where the horizontal velocity $U(\tilde{x})$ has the asymptotic behaviours

$$U \sim W_0\tilde{x}, \ \tilde{x} \to 0, \quad U \to 1, \ \tilde{x} \to \infty. \tag{6.9}$$

Near the origin the solution of (6.4)–(6.7) is equivalent to a stagnation point flow $\tilde{\Phi} \sim W_0\tilde{x}\tilde{\zeta}$.

6.2. *Conductive sublayer*

Between the convective zone and the vertical wall there is a conductive sublayer (figure 5, region VII), the continuation of the inner zone of the vertical boundary layer. Here

$$\left.\begin{aligned} T &= \{b + R^{-1/4}L^{1/2}b_0 + \cdots\} + R^{-5/8}L^{-1/4}\lambda_0^{1/4}\tilde{T}(\tilde{\xi},\tilde{\zeta}) + \cdots, \\ \psi &= R^{1/16}L^{1/8}\lambda_0^{1/8}\tilde{\psi}(\tilde{\xi},\tilde{\zeta}) + \cdots, \end{aligned}\right\} \tag{6.10}$$

as $R \to \infty$, where $x = R^{-7/16}L^{1/8}\lambda_0^{-3/8}\tilde{\xi}$, and from (2.3) the functions $\tilde{\psi}$ and $\tilde{T}$ satisfy

$$\frac{\partial^2\tilde{\psi}}{\partial\tilde{\xi}^2} = 0, \quad \frac{\partial^2\tilde{T}}{\partial\tilde{\xi}^2} = \frac{\partial(\tilde{T},\tilde{\psi})}{\partial(\tilde{\xi},\tilde{\zeta})}. \tag{6.11}$$

Matching with the convective zone and satisfaction of the wall condition $\tilde{\psi} = 0$ at $\tilde{\xi} = 0$ gives

$$\tilde{\psi} = W(\tilde{\zeta})\tilde{\xi}. \tag{6.12}$$

The solution for $\tilde{T}$ satisfying the wall condition $\partial\tilde{T}/\partial\tilde{\xi} = 0$ at $\tilde{\xi} = 0$, with the behaviour $\tilde{T} \sim k\tilde{\psi}^2$ as $\tilde{\xi} \to \infty$ needed to match with the convective zone, and which matches with the inner zone of the vertical boundary layer as $\tilde{\zeta} \to \infty$, is

$$\tilde{T} = k\left(W^2(\tilde{\zeta})\tilde{\xi}^2 - 2\int_0^{\tilde{\zeta}} W(\tilde{\zeta})\mathrm{d}\tilde{\zeta}\right). \tag{6.13}$$

Within this sublayer the wall temperature undergoes an adjustment from the cubic form $\tilde{T} \sim -2k^2\tilde{\zeta}^3/3$ as $\tilde{\zeta} \to \infty$, consistent with (5.49), to the quadratic form $\tilde{T} \sim -kW_0\tilde{\zeta}^2$ as $\tilde{\zeta} \to 0$.

6.3. *Transitional layer*

Beneath the convective zone there is a region where the stable stratification develops and the entrainment velocity decays to exponentially small values. Within this transitional layer (figure 5, region VIII),

$$\left.\begin{aligned} T &= \{b + R^{-1/4}L^{1/2}b_0 + \cdots\} + R^{-7/16}L^{1/8}\lambda_0^{5/8}\tilde{\theta}(\tilde{x},\tilde{z}) + \cdots, \\ \psi &= R^{1/16}L^{1/8}\lambda_0^{1/8}\tilde{\phi}(\tilde{x},\tilde{z}) + \cdots, \end{aligned}\right\} \tag{6.14}$$

as $R \to \infty$, where

$$\zeta = \zeta_0 - R^{-3/16}L^{-3/8}\lambda_0^{-3/8}\tilde{z} \tag{6.15}$$

and $\tilde{\theta}$ and $\tilde{\phi}$ satisfy the horizontal boundary layer equations

$$\frac{\partial^2\tilde{\phi}}{\partial\tilde{z}^2} = -\frac{\partial\tilde{\theta}}{\partial\tilde{x}}, \quad \frac{\partial^2\tilde{\theta}}{\partial\tilde{z}^2} = \frac{\partial(\tilde{\theta},\tilde{\phi})}{\partial(\tilde{x},\tilde{z})}, \tag{6.16}$$

with boundary conditions

$$\tilde{\phi} \sim U(\tilde{x})\tilde{z},\ \tilde{\theta} \to 0 \ \text{ as } \tilde{z} \to \infty, \quad \tilde{\phi} \to 0,\ \tilde{\theta} \sim \tilde{z} \ \text{ as } \tilde{z} \to -\infty, \tag{6.17}$$

$$\tilde{\phi} = \frac{\partial\tilde{\theta}}{\partial\tilde{x}} = 0 \ \text{ on } \tilde{x} = 0. \tag{6.18}$$

Here (6.17) follow from matching with the convective zone and from the assumption of a stratified region of weak motion beneath the transitional layer, whilst (6.18) assumes that the solution satisfies the wall conditions at $\tilde{x} = 0$; the wall temperature $\tilde{\theta}(0,\tilde{z})$ is to be determined as part of the solution. Integration of the second equation in (6.16) and use of (6.17), (6.18) shows that the solution of (6.16)–(6.18) satisfies the integral relation

$$\int_{-\infty}^{\infty} \tilde{\phi}\frac{\partial\tilde{\theta}}{\partial\tilde{z}}\mathrm{d}\tilde{z} = \tilde{x} \tag{6.19}$$

for all $0 \leqslant \tilde{x} < \infty$, and it is easily established that as $\tilde{x} \to \infty$ the solution approaches the transitional structure of the outer horizontal boundary layer near ζ_0 identified in § 5.2, with

$$\tilde{\phi} \sim \tilde{x}^{1/2}\tilde{f}(\tilde{\beta}), \quad \tilde{\theta} \sim \tilde{x}^{1/2}\tilde{g}(\tilde{\beta}) \ \text{ as } \tilde{x} \to \infty, \tag{6.20}$$

where $\tilde{g} = \tilde{\beta}\tilde{f} - \tilde{f}$, $\tilde{\beta} = \tilde{z}/\tilde{x}^{1/2}$ and $\tilde{f}$ is the solution (5.41) with $b_1 = 0$:

$$\tilde{f} = \frac{\tilde{\beta}}{2}\left(1 + \mathrm{erf}\frac{\tilde{\beta}}{2}\right) + \frac{1}{\sqrt{\pi}}\mathrm{e}^{-\tilde{\beta}^2/4}. \tag{6.21}$$

As $\tilde{x} \to 0$, the solution can be expanded in the form

$$\tilde{\theta} = \tilde{\theta}_0(\tilde{z}) + \tilde{x}^2\tilde{\theta}_2(\tilde{z}) + \cdots, \quad \tilde{\phi} = \tilde{x}\tilde{\phi}_1(\tilde{z}) + \tilde{x}^3\tilde{\phi}_3(\tilde{z}) + \cdots, \tag{6.22}$$

with successive terms determined from (6.16) in terms of the unknown temperature $\tilde{\theta}_0(\tilde{z})$ at $\tilde{x} = 0$. Thus

$$\tilde{\phi}_1 = -\tilde{\theta}_0''/\tilde{\theta}_0', \quad \tilde{\theta}_2 = -\tilde{\phi}_1''/2, \quad \tilde{\phi}_3 = (2\tilde{\phi}_1'\tilde{\theta}_2 - \tilde{\phi}_1\tilde{\theta}_2' - \tilde{\theta}_2'')/3\tilde{\theta}_0', \cdots. \tag{6.23}$$

A numerical solution of (6.16)–(6.18) was obtained by inserting time derivatives $\partial\tilde{\phi}/\partial t$ and $\partial\tilde{\theta}/\partial t$ on the right-hand sides of (6.16) and allowing the solution to evolve to its steady form from an initial state taken as

$$\tilde{\phi} = U(\tilde{x})\tilde{x}_\infty^{1/2}\tilde{f}(\tilde{z}/\tilde{x}_\infty^{1/2}), \quad \tilde{\theta} = \tilde{x}_\infty^{1/2}\tilde{g}(\tilde{z}/\tilde{x}_\infty^{1/2}) \ \text{ at } t = 0. \tag{6.24}$$

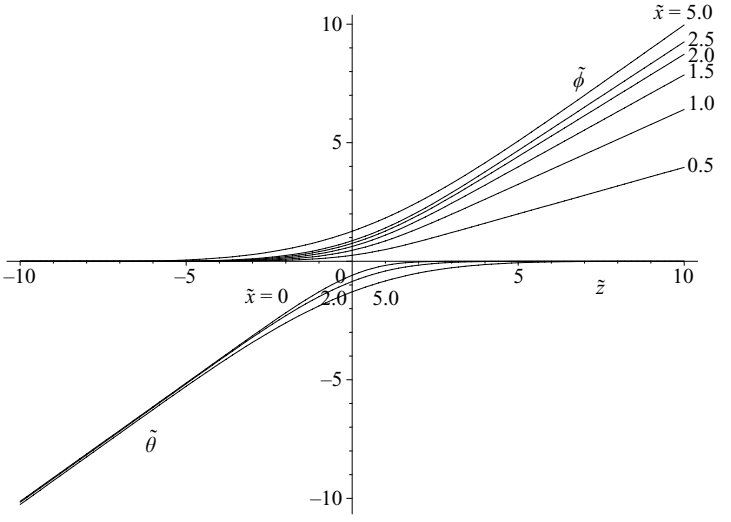

FIGURE 8. Profiles of $\tilde{\theta}$ and $\tilde{\phi}$ in the transitional layer for various values of $\tilde{x}$.

The equations were discretized using central differences in $\tilde{x}$ and $\tilde{z}$ on the numerical domain $0 \leqslant \tilde{x} \leqslant \tilde{x}_\infty$, $-\tilde{z}_\infty \leqslant \tilde{z} \leqslant \tilde{z}_\infty$ and a forward difference in time; checks on accuracy were made with various outer boundaries and step sizes.

Results for outer boundaries $\tilde{x}_\infty = 10$, $\tilde{z}_\infty = 12$ with step sizes $\Delta\tilde{x} = 0.1$, $\Delta\tilde{z} = 0.2$ and $\Delta t = 10^{-3}$ are shown in figure 8 for the case where $U(\tilde{x}) = 1 - \mathrm{e}^{-\tilde{x}}$. In this case a converged solution was achieved when t reached a value of approximately 400. One difficulty encountered was that in the region of very weak flow near $-\tilde{z}_\infty$, slightly negative values of $\tilde{\phi}$ were generated which eventually led to instability; this was countered by replacing such values of $\tilde{\phi}$ by zero at each time step, so that effectively the outer boundary $\tilde{z} = -\tilde{z}_\infty$ was replaced by a boundary which increased in magnitude with $\tilde{x}$. A large value of $\tilde{z}_\infty$ is essential to capture the spread of the solution with $\tilde{x}$, and an alternative remedy (which was not attempted) would be to carry out the computation on an appropriate non-uniform grid or to use a coordinate transformation of the equations to reflect the structure of the solution (that is, with $\tilde{z} \sim 1$ as $\tilde{x} \to 0$ and $\tilde{z} \sim \tilde{x}^{1/2}$ as $\tilde{x} \to \infty$). The numerical results confirmed the emergence of the asymptotic form (6.20) as $\tilde{x} \to \infty$.

At the junction of the conductive sublayer and the transitional layer where $\tilde{z}$ and $\tilde{\xi}$ are finite (figure 5, region IX), the solution is given by

$$T = \{b + R^{-1/4}L^{1/2}b_0 + \cdots\} + R^{-7/16}L^{1/8}\lambda_0^{5/8}\hat{T}(\tilde{\xi}, \tilde{z}) + \cdots, \quad \psi = \hat{\psi}(\tilde{\xi}, \tilde{z}) + \cdots, \tag{6.25}$$

and in the governing equations (2.3) the term $\nabla^2\psi$ is neglected at leading order. Thus $\hat{T}$ is independent of $\tilde{\xi}$ and the solution is simply a continuation of the leading terms in the transitional layer solution as $\tilde{x} \to 0$:

$$\hat{T} = \tilde{\theta}_0(\tilde{z}), \quad \hat{\psi} = -\tilde{\theta}_0''\tilde{\xi}/\tilde{\theta}_0'. \tag{6.26}$$

This completes a leading-order description of the solution structure throughout the cavity in the limit as $R \to \infty$.

7. Discussion

An asymptotic structure in the limit as $R \to \infty$ has been described for thermally driven cavity flow in a porous medium where a stable uniformly stratified state is modified by a monotonic horizontal temperature differential at the upper boundary. At the upper surface there is an inner horizontal boundary layer of depth order $R^{-1/3}$, where the temperature adjusts to a constant value somewhat larger than the minimum temperature at the upper surface. A second adjustment then takes place in an outer horizontal layer over a depth of order $R^{-1/4}$ where the vertical thermal gradient adjusts to its uniform value, λ. Solutions in the two horizontal layers depend on the interaction with the vertical boundary layer near the colder sidewall. The width of this layer increases with depth until the layer eventually terminates at a stagnation point on the wall where the wall temperature reaches a maximum value. This occurs at a finite depth measured on the vertical scale of the outer horizontal layer, this depth being determined by the relation (5.50) between the horizontal flow speed and the square root of the vertical temperature gradient. This allows a local transition from flow to stratification to occur. The influence of the vertical thermal gradient λ is shown, via a heat flux integral argument, to extend to the first correction terms in the outer horizontal layer solution as $\zeta \to 0$; this in turn generates corrections of relative order $R^{-1/3}$ within the inner horizontal layer.

A full solution of the outer horizontal/vertical layer problem defined by (5.3)–(5.6), (5.8)–(5.12) and (5.15) requires a numerical approach that takes account of the singular structure of the solution not only as $\zeta \to 0$ but also as $\zeta \to \zeta_0$ and $X \to 0$. It also requires an interactive treatment of the horizontal and vertical layers, allowing the terminal point ζ_0 to be determined. In such a solution it would be possible to exploit the fact that the parameter λ can be eliminated by rescaling the temperatures, streamfunctions and coordinates ξ and ζ with $\lambda^{3/4}$, $\lambda^{1/4}$, $\lambda^{-1/2}$ and $\lambda^{-1/4}$ respectively. In particular, the terminal point ζ_0 has the form $\zeta_0 = \lambda^{-1/4}\hat{\zeta}_0$ where $\hat{\zeta}_0$ is a pure number, which from (5.2) is equivalent to

$$z \sim 1 - \hat{\zeta}_0 \lambda^{-1/4} L^{1/2} R^{-1/4} + D L^{2/3} R^{-1/3}, \quad R \to \infty. \tag{7.1}$$

A numerical solution of the outer problem to find ζ_0 is not attempted here, and the estimate $\zeta_0 = 1.418\lambda^{-1/4}$ given by the small-ζ analysis of § 5.1 is too low, the corresponding value of $-\Phi'_\infty(\zeta_0) = 12.74\lambda^{1/2}$ being much higher than that needed to satisfy the terminal condition (5.50), $-\Phi'_\infty(\zeta_0) = \lambda_0^{1/2}$. In practice this condition imposes a higher value of ζ_0, which can be estimated by approximating λ_0 by λ and writing $\Phi_\infty(\zeta) = \lambda^{1/4}\hat{\Phi}_\infty(\hat{\zeta})$ where $\zeta = \lambda^{-1/4}\hat{\zeta}$. The function $\hat{\Phi}_\infty$ must then satisfy $\hat{\Phi}_\infty \sim p_0 \hat{\zeta}^{-1}$ as $\hat{\zeta} \to 0$, $\hat{\Phi}_\infty(\hat{\zeta}_0) = 0$ and $\hat{\Phi}'_\infty(\hat{\zeta}_0) = -1$. For an interpolation based on a suitable class of cotangent functions $\hat{\Phi}_\infty = A\cot(B\hat{\zeta})$, it follows that $A = B^{-1} = p_0^{1/2}$ and the terminal point is determined as $\hat{\zeta}_0 = \pi p_0^{1/2}/2 = 3.97$. This approximation to $\hat{\Phi}_\infty$ can be improved to allow for the correction terms of order $\hat{\zeta}^3$ in $\hat{\Phi}_\infty$ as $\hat{\zeta} \to 0$ by incorporating a multiplicative function of $\hat{\zeta}$ that approaches unity as $\hat{\zeta}$ tends to 0 and $\hat{\zeta}_0$.

A comparison of (7.1) with numerical computations requires consideration of the transitional layer centred on ζ_0 where the motion adjacent to the cold sidewall finally succumbs to the stable stratification. The transformation from flow to stratification is illustrated by the transitional layer profiles in figure 8, and can be observed in figures 2 and 3 as a transition from near-horizontal streamlines to near-horizontal isotherms. According to the asymptotic theory, the upper limit of the transitional layer is associated with the wall temperature attaining its maximum value, whilst the lower limit is associated with the stagnation point. This is consistent with the

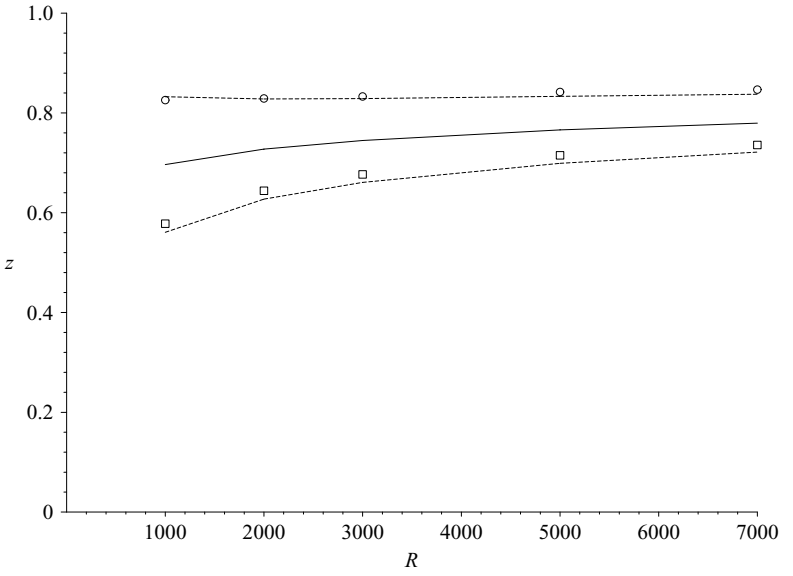

FIGURE 9. Comparison of the asymptotic theory with numerical results for the case $\tau = -1, L = 1$ and values of R from 1000 to 7000 showing the terminal height z of the vertical boundary layer predicted by (7.1) (—), the vertical extent of the transitional layer predicted by (6.15) with $\tilde{z} = \pm 3$ (- - -) and numerical results for the height of the upper stagnation point (□) and maximum wall temperature (o).

behaviours in figures 2 and 3 and explains why the maximum wall temperature and stagnation point do not coincide in practice, even though, on the scale of the vertical boundary layer, they occur at the same location $\zeta = \zeta_0$. Figure 9 shows the height of the maximum wall temperature and of the stagnation point given by numerical computations for the case $L = 1, \tau = -1$ and a range of values of R up to 7000. The gradual convergence with increasing R is consistent with the asymptotic theory and in particular with the terminal height of the vertical boundary layer predicted by (7.1) with $\lambda = b - \tau = 1.213$, $D = 3.70$ and $\hat{\zeta}_0 = 3.97$, also shown in figure 9. It is also consistent with the vertical extent of the transitional layer as given by (6.15) with upper and lower boundaries taken at $\tilde{z} = \pm 3$ and λ_0 approximated by λ; this too is shown in figure 9. An increase of $\hat{\zeta}_0$ to 5 or a decrease to 3 moves the asymptotic curve of the terminal height outside the numerical data in figure 9, suggesting that the estimate of $\hat{\zeta}_0$ as 3.97 is a reasonable one.

Another test of the present theory concerns the prediction of the depth of the weak convection cells in the lower part of the cavity. The analysis of § 5.3 predicts the cell depth between zero streamlines to be

$$z = z_d \sim \sqrt{2\pi}\lambda^{-1/4} L^{1/2} R^{-1/4}, \quad R \to \infty. \tag{7.2}$$

Figure 10 shows a comparison of this formula with numerical results for $L = 1, \tau = -1$ and values of R up to 7000; excellent agreement is obtained, confirming both the power-law dependence on R and the multiplicative factor in formula (7.2).

The vertical temperature gradient in the lower part of the cavity is predicted to approach the value λ as $R \to \infty$. This is consistent with the trend of the values 1.44 and 1.39 in figures 2 and 3 respectively, and a gradual approach to the value 1.213

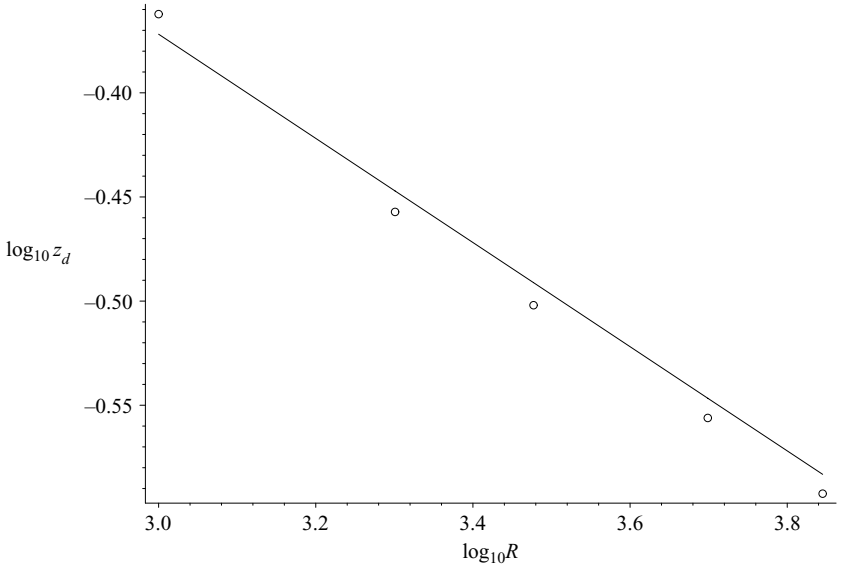

FIGURE 10. Comparison of the asymptotic theory with numerical results for the case $\tau = -1, L = 1$ and values of R from 1000 to 7000 showing a logarithmic plot of the cell depth z_d of the convection cell immediately below the main cell, as predicted by (7.2) (—) and numerical computation (o).

from above is to be expected given that in practice the change from τ to b occurs over the region below the inner horizontal layer rather than over the full cavity depth.

In terms of applications, the result (7.1) is of interest in that it defines the critical depth to which the upper surface circulation extends. This is significant in predicting the extent of the near-surface spread of pollution in groundwater, for example from groundfill sites and from industrial waste discharge in coastal and river-bed systems. The upper surface temperature profile influences the critical depth through the value of D in the $R^{-1/3}$ term in (7.1) and, primarily, through the value of b which, along with the lower surface temperature τ, determines the value of λ in the $R^{-1/4}$ term. The critical depth is thus completely determined by λ, D, the Darcy–Rayleigh number R and the aspect ratio L. For large (negative) lower surface temperatures τ of order $R^{1/3}L^{-2/3}$, the upper surface temperature has a more direct influence because the inner and outer horizontal layers merge to form a single horizontal layer of depth $R^{-1/3}L^{2/3}$, and the two terms in (7.1) then have the same order of magnitude. The resulting modified boundary layer problem is to solve the inner system (4.2)–(4.5), (4.7)–(4.11), but with the thermal condition in (4.5) replaced by $\partial\bar{\theta}/\partial Z \to -\bar{\lambda}$ as $Z \to \infty$, where $\bar{\lambda} = \lambda R^{-1/3}L^{2/3}$ is a finite parameter. The terminal point of the vertical boundary layer then occurs at a finite value of Z that depends on both $\bar{\lambda}$ and the upper surface temperature profile.

The author acknowledges the helpful comments of referees.

Appendix. Vertical boundary layer structure as $\zeta \to \zeta_0$

Suppose that the outer forms (5.36) apply with both a_1 and b_1 non-zero. This would require a solution in the vertical boundary layer of the form

$$\Phi = (\zeta_0 - \zeta) f(\xi) + \cdots, \quad \Theta = b_0 + (\zeta_0 - \zeta) g(\xi) + \cdots,$$

as $\zeta \to \zeta_0-$, in place of (5.43). From (5.8), $g = b_1 - f'$ and f satisfies the equation

$$f''' - ff'' + f'(f' - b_1) = 0.$$

The exact solution with the required behaviour as $\xi \to \infty$ is

$$f = a_1 + c_1 \exp\left\{ - \left(\left(a_1^2 + 4b_1\right)^{1/2} - a_1\right)\xi/2\right\},$$

where c_1 is an arbitrary constant. However, this cannot satisfy the two wall conditions $f = f'' = 0$ at $\xi = 0$ unless $b_1 = 0$, in which case the solution for f is null. An implication is that the outer temperature field is of smaller magnitude as $\zeta \to \zeta_0$, leading to the structure described in § 5.2.

REFERENCES

Chang, I. D. & Cheng, P. 1983 Matched asymptotic expansions for free convection about an impermeable horizontal surface in a porous medium. *Intl J. Heat Mass Transfer* **26**, 163–173.

Cheng, P. & Chang, I. D. 1976 On buoyancy induced flows in a saturated porous medium adjacent to impermeable horizontal surfaces. *Intl J. Heat Mass Transfer* **19**, 1267–1272.

Daniels, P. G. 2006 Shallow cavity flow in a porous medium driven by differential heating. *J. Fluid Mech.* **565**, 441–459.

Daniels, P. G., Blythe, P. A. & Simpkins, P. G. 1982 Thermally driven cavity flows in porous media. Part II. The horizontal boundary-layer structure. *Proc. R. Soc. Lond.* A **382**, 135–154.

Daniels, P. G. & Punpocha, M. 2004 Cavity flow in a porous medium driven by differential heating. *Intl J. Heat Mass Transfer* **47**, 3017–3030.

Daniels, P. G. & Punpocha, M. 2005 On the boundary-layer structure of cavity flow in a porous medium driven by differential heating. *J. Fluid Mech.* **532**, 321–344.

Tayler, A. B. 1986 *Mathematical Models in Applied Mechanics*. Clarendon.

Weber, J. E. 1975 The boundary-layer regime for convection in a vertical porous layer. *Intl J. Heat Mass Transfer* **18**, 569–573.